Available online at www.sciencedirect.com
ScienceDirect
Journal of Nuclear Materials 367–370 (2007) 483–488
journal of nuclear materials
www.elsevier.com/locate/jnucmat

Thermal helium desorption spectrometry of helium-implanted iron

Donghua Xu *, Tjacka Bus, Stephen C. Glade, Brian D. Wirth

Department of Nuclear Engineering, University of California, Berkeley, CA 94720, USA

Abstract

Thermal helium desorption spectrometry (THDS) is employed to study the kinetics and energetics of helium in iron implanted with 100 keV He to 1×10^{11}, 1×10^{13}, and 1×10^{15} He/cm^2. While no clear desorption signals are observed for the two lower dose samples, preliminary results reveal that the majority of the He atoms desorb at ~1000 °C and at >1100 °C for the 1×10^{15} He/cm^2 sample. Both conventional reaction model and Johnson–Mehl–Avrami (JMA) transformation model are utilized to analyze the ~1000 °C desorption event. The measured signal can be reproduced very well by combining a first-order and a higher order ($n\sim5.8$) JMA fits. This event is observed repetitively during successive heating–cooling cycles. The success of the higher order JMA model and the repetitive appearance strongly suggest that this event is mainly associated with $\alpha\leftrightarrow\gamma$ phase transformation, while the dissociation of HeV clusters may also be involved. The observation of spurious peaks which may affect future studies is also reported.

1. Introduction

The development of fusion reactors requires knowledge of material behavior in the fusion environment, in particular with regard to high levels of helium produced by (n,α) reactions. It has been established that implanted or internally produced He can cause significant mechanical property degradation [1–5]. A crucial aspect, therefore, is to understand how helium atoms migrate and are trapped by microstructural features in irradiated materials. While a large amount of theory, modeling and experimental research has been performed in the past years, the understanding of this problem is still far from complete. Thermal helium desorption spectrometry (THDS) has been employed to experimentally study irradiation-induced structural defects and their interactions with He atoms in a variety of materials. For example, nucleation and growth of He–vacancy clusters were reported in vanadium and vanadium alloys [6], and the sequential release of interstitial He and He–vacancy clusters was reported in SiC [7] based on the THDS spectra.

In iron and ferritic alloys, computer simulations have been performed on defect production in collision cascades caused by helium injection [8], effect of He–vacancy complexes on mechanical properties [9], thermal stability of He–vacancy clusters in iron [10], He–grain boundary interaction [11] and defect evolution in iron during annealing after electron irradiation [12]. Experimentally, nuclear reaction depth profiling [13], transmission electron microscopy

* Corresponding author.
E-mail addresses: xudh@nuc.berkeley.edu (D. Xu), bdwirth@nuc.berkeley.edu (B.D. Wirth).

0022-3115/$ - see front matter © 2007 Elsevier B.V. All rights reserved.
doi:10.1016/j.jnucmat.2007.03.112

[14], positron annihilation lifetime and coincidence Doppler broadening (CDB) techniques [15,16] have been used in addition to THDS [10, 17,18] to study He migration and He-induced defect clusters in iron. In addition, resistivity recovery measurement has been used to study kinetics of defects in iron produced by electron irradiation [19].

In this work, we use THDS to study the kinetics and energetics of helium in iron implanted with 100 keV He to three different doses, 1×10^{11}, 1×10^{13}, and 1×10^{15} He/cm^2. Constant heating rate ramps are employed to thermally desorb the implanted He. The resulting desorption signals are analyzed with both conventional reaction model and Johnson–Mehl–Avrami (JMA) transformation model kinetics. Spurious desorption peaks and repetitive appearance of a characteristic desorption event during successive heating–cooling cycles are reported. Potential mechanisms for the observed desorption are briefly discussed.

2. Experimental

In our THDS system recently built at UC Berkeley [20], both the sample chamber and the measurement (quadrupole mass spectrometer) chamber are maintained at ultra-high vacuum with a pressure of about 10^{-10} Torr (at room temperature). The He, as well as other species (N_2, H_2, etc.), is detected by the mass spectrometer (maintained at room temperature) while the sample is heated according to a desired temperature profile.

A THDS system can be operated in either static (no pumping during a measurement) or dynamic mode (gas being constantly pumped out during a measurement). In this study, the dynamic mode was employed to prevent accumulation of desorbed He in the measurement chamber. In the dynamic mode with a fixed chamber volume V, assuming He at room temperature T_r, the He pressure inside the chamber P, as seen by the mass spectrometer, is governed by the differential equation $V\mathrm{d}P = K_B T_r \mathrm{d}\overline{N} - \frac{PV}{\tau}\mathrm{d}t$, in which τ is a pumping time constant, and $\mathrm{d}\overline{N}$ is the number of He atoms desorbed from the sample in the time period of $\mathrm{d}t$. If τ is very small such that $\mathrm{d}P/\mathrm{d}t \ll P/\tau$,[1] then one obtains $\mathrm{d}\overline{N}/\mathrm{d}t \propto P$. However, as will be shown and discussed later, even when τ is indeed negligible, some non-negligible spurious signals (even peaks) which apparently do not result from the desorption of implanted He may still contribute to the measured pressure P. Therefore, a more careful expression should be: $\mathrm{d}\overline{N}/\mathrm{d}t \propto (P - P_{base})$ where P_{base} can be regarded as the signal measured from an otherwise-similar but non-implanted control sample.

The calibration factor for the mass spectrometer was determined to be $\sim5.5\times10^{-22}$ C/He-atom. Polycrystalline iron plates of 1 mm thickness with a purity of 99.5% were purchased from Goodfellow and then commercially implanted with 100 keV helium to three different doses: 1×10^{11}, 1×10^{13}, and 1×10^{15} He/cm^2. Constant rate heating ramps of 0.5 K/s and 1 K/s were used for both the control and the actual desorption measurements.

3. Results and discussion

3.1. TRIM/SRIM calculations

The damage (displacement per iron atom at varying depth), He distribution, vacancy/He ratio and other factors related to He implantation in Fe were calculated with SRIM 2003 software [21]. For 100 keV He implantation, the vacancy/He ratio is 87 and the peak He concentration for a dose of 1×10^{15} He/cm^2 is about 700 appm at a depth of 340 nm.

3.2. Spurious peaks

A comparison between two samples: S10 (1×10^{15} He/cm^2 dosed) and S12 (non-implanted control) is shown in Fig. 1(a). The same heating control parameters were used for both samples which produced almost identical actual temperature profiles during the measurements. Fig. 1(a) shows that both samples exhibit a set of medium temperature He peaks in the range of ~600–880 °C, and, more importantly, the positions of these medium temperature peaks are almost identical for the two samples. However, the implanted sample S10 displays much stronger signals than the non-implanted S12 at temperatures higher than ~880 °C, including a fully developed peak around 1017 °C and a broad peak with an onset of ~1130 °C.

Apparently, the medium temperature peaks in the range of ~600–880 °C are not due to the desorption of implanted He, and thus are referred to as spurious peaks (signals) throughout this paper.

[1] The accuracy of this assumption can be checked during data analysis by numerically comparing these two terms. τ can be found in calibration procedure. In this work, $\tau = 0.3$ s and the assumption is sufficiently satisfied.

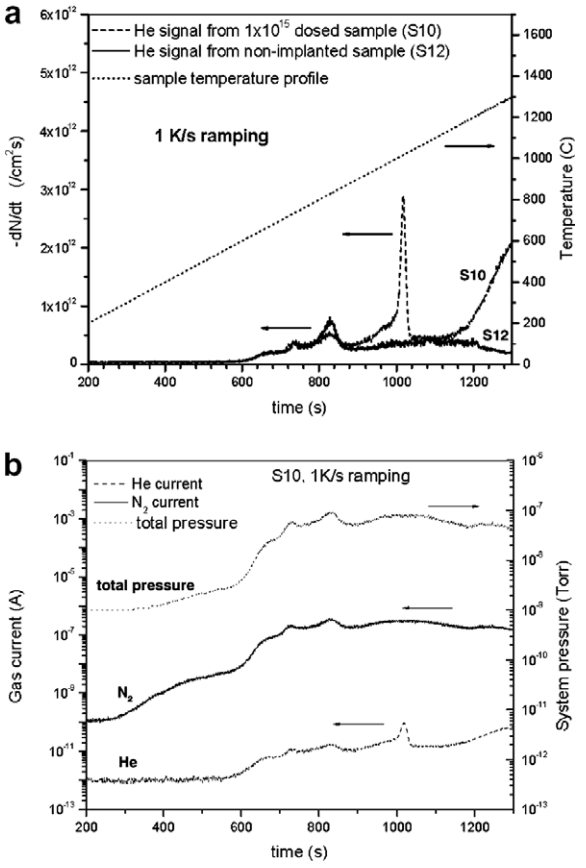

Fig. 1. (a) Comparison between He signals measured from two samples, S10 (1×10^{15} He ions/cm^2) and S12 (non-implanted) and (b) correlations among He signal, other gas signals (represented by N_2), and total system pressure, measured from sample S10 – note that a logarithmic scale is used.

The real identifiable desorption events start from above 880 °C in the 1 K/s ramping measurement of S10. Since the magnitudes of the spurious peaks are not negligible compared with the real desorption peaks, it is crucial to perform a control analysis before making peak assignments, particularly if the He desorption under consideration occurs in a relatively low temperature range (e.g., below 880 °C). Whether such spurious peaks also contributed to the observed signals in previous THDS studies is unclear.

While the exact origin of the spurious peaks is still under investigation, they appear to be related to the desorption of non-implanted gas species from internal components such as filament and thermal shields as well as from sample surface. As shown in Fig. 1(b), other channels of the mass spectrometer, such as N_2, as well as the total system pressure, also exhibit peaks at basically the same temperatures.[2] Moreover, even a copper gasket was found to exhibit similar peaks on all channels of the mass spectrometer (including He) at relatively lower temperatures from 500 to 750 °C. It must also be noted that all these spurious peaks do not appear when an empty-chamber (without any sample) is measured, indicating system cleanliness is not the sole reason. It appears that surface contamination of the sample may also be partly responsible for the spurious peaks.

3.3. Samples of 1×10^{15} He/cm^2 dose

3.3.1. Reaction model analysis

From the 1 K/s (β_1) constant rate ramping data presented in Fig. 1(a) (dashed line), the peak temperature T_p of the first desorption event of the 1×10^{15} He/cm^2 dosed iron was determined to be 1017 °C. The ramping measurement was also performed at a heating rate of 0.5 K/s (β_2), which shifted the T_p to 993 °C.

A number of previous studies (e.g., [22]) have assumed that He desorption obeys a first-order chemical reaction model, i.e., $dN/dt = -K_0 \exp(-Q/K_B T)*N$, where N is the number of remaining He atoms in the sample corresponding to a given desorption event, K_0 is a frequency factor, Q is the activation energy of the desorption event, and K_B is the Boltzmann constant. By solving the equation $d^2N/dt^2 = 0$ under the constant rate ramping condition (i.e., $dT/dt = \beta$), it can be shown that the peak temperature T_p on the dN/dt signal satisfies the equation $\ln(\beta/T_p^2) = -Q/K_B T_p + \ln(K_0 K_B/Q)$. Therefore, the use of two sets of T_p vs. β data can determine both the activation energy Q and the frequency factor K_0. In this case, we obtain $Q = 3.8$ eV and $K_0 = 2.04 \times 10^{13}$/s. Nevertheless, as shown in Fig. 2, a back-calculation of dN/dt using these parameters and the assumed first-order-reaction model does not provide satisfactory agreement with the experimental peak, particularly with respect to the peak sharpness (half-maximum width) and steepness. Moreover, even when Q and K_0 are allowed to vary around these values (3.8 eV and 2.04×10^{13}/s), similar fits are obtained and the sharpness of the entire event still cannot be adequately described.

[2] These other channels are distinguished from the He channel at temperatures higher than ~880 °C where the implanted He clearly starts to desorb. Note that a logarithmic scale is used in Fig. 1(b) for comparison of different channels.

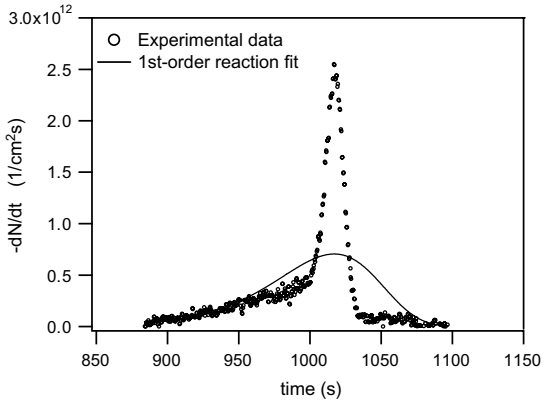

Fig. 2. First-order fit using reaction model for the 1017 °C desorption event of the 1×10^{15} He ions/cm^2 dosed sample: $n = 1$, $Q = 3.81$ eV, $K_0 = 2.04 \times 10^{13}$/s.

A non-1st-order reaction model was then considered in an attempt to obtain better agreement with the experimental data. From the general form of the reaction model, i.e., $dN/dt = -K_0\exp(-Q/K_BT) * N^n$ (where n is the order of reaction), one can obtain: $d^2N/dt^2 = dN/dt * [\beta Q/(K_BT^2) + (n/N) * dN/dt]$. Therefore, at the peak temperature, $Q/n = -[K_BT_p^2/(\beta * N_p)] * \frac{dN}{dt}|_p$, where N_p can be numerically determined using the measured dN/dt data. Hence, Q/n is determined to be 15.8 eV for the 1017 °C desorption event, and then $dN/dt = -K_0[N * \exp(-15.8/K_BT)]^n$. If the general form of the reaction model is a good description of the event, the plot of $\ln(-dN/dt)$ vs. $\ln[N * \exp(-15.8/K_BT)]$ should be close to a straight line with a slope of n and an intercept of $\ln K_0$. However, the plot of the 1017 °C event obeys this linearity only at the early stage (up to 1000 s, i.e., 1000 °C) of the event, and significantly deviates thereafter, indicating the inadequacy of this general reaction model for the description of this event.

3.3.2. Johnson–Mehl–Avrami (JMA) model analysis

A JMA kinetic model [23,24] was then employed to analyze the desorption event at $T_p = 1017$ °C. The general form of the JMA model can be written as: $x = 1 - \exp(-K^nt^n)$, where $K = K_0\exp(-Q/K_BT)$, x is the transformed (in this case, desorbed) fraction of He atoms corresponding to a certain event, i.e., $x \equiv 1 - N(t)/N_0$. Therefore, the desorption rate can be derived as: $dN/dt = -N_0dx/dt = -N_0 * nK^nt^{n-1}\exp(-K^nt^n) * [1 + \beta tQ/(K_BT^2)]$ for constant rate ramps. According to Henderson's analysis (Appendix A7 in Ref. [25]), the activation energy Q in this model[3] can be approximated using the peak shifting approach, i.e., $Q \approx$ slope of $\ln(\beta/T_p^2)$ vs. $-1/K_BT_p$.[4] Analysis of the two sets of T_p vs. β data presented earlier results in $Q \approx 3.8$ eV. Thus, we fixed Q to this value and varied n and K_0 to obtain a series of fits for the desorption signal, four of which are shown in Fig. 3. As was the case with the first-order-reaction fit, the first-order JMA fit cannot describe the sharpness of the desorption peak. However, as the order n increases, the JMA fit becomes sharper and the fit-peak increases such that it better reproduces the experimental peak. On the other hand, a higher order (e.g. $n = 4$) JMA fit cannot adequately describe the early stage ($t < 1000$ s) of the experimental signal.

The fact that neither the first-order, nor a single higher order fit can satisfactorily account for the entire signal leads to the hypothesis that more than one single-order event is involved. Indeed, as shown in Fig. 4, by combining a low order component with a high order component within the JMA model (see the Appendix for fitting methodology), the entire signal can be reproduced very well. The fit result suggests that ~44% of the total He atoms involved in this entire event desorb according to a low order ($n \sim 1.1$) in the early stage and the remaining 56% desorb with a higher order ($n \sim 5.8$). It should be emphasized that the low order component can also be reproduced very well using the reaction model although the high order component can only be described using the JMA model.

3.3.3. Repetitive appearance of the ~1000 °C desorption event

The above analyses are based on the desorption signal recorded during the first heating ramp of a sample. However, this characteristic event (its sharp component, to be exact) at ~1000 °C was also observed during immediate cooling following the first heating and even during subsequent heating–cooling cycles. Only after a sample was annealed isothermally at a very high (1330 °C) temperature for a long time (~30 min) did the event disappear completely during subsequent heatups and cooldowns.

[3] Note that Q here is equivalent to the $\Delta H/n$ in Henderson's analysis, and K_0 here is equivalent to Henderson's $K_0^{1/n}$.

[4] This is essentially the same technique used for determination of the activation energy in the 1st-order reaction analysis. However, the intercepts in the two analyses are different.

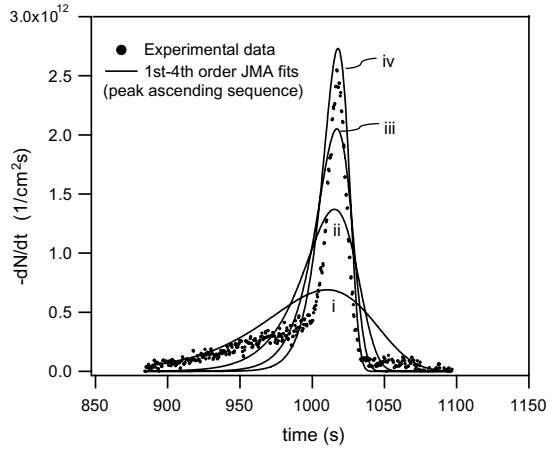

Fig. 3. Single-order JMA fits for the 1017 °C desorption event of the 1×10^{15} He ions/cm^2 dosed sample, with fixed activation energy $Q=3.81$ eV, and varied n and K_0 (in the peak ascending sequence): (i) $n=1$ and $K_0=8.6\times10^{11}$/s; (ii) $n=2$ and $K_0=7.8\times10^{11}$/s; (iii) $n=3$ and $K_0=7.5\times10^{11}$/s; and (iv) $n=4$ and $K_0=7.4\times10^{11}$/s.

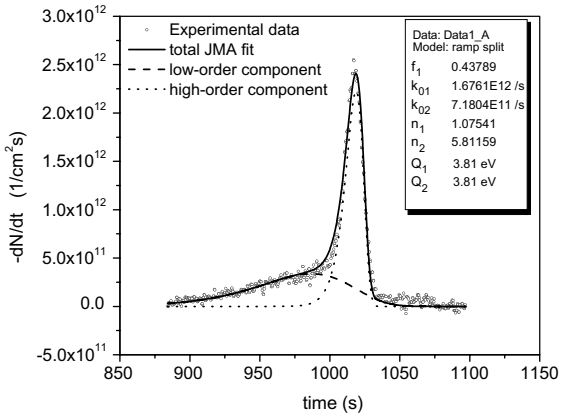

Fig. 4. Combined JMA fit for the 1017 °C desorption event of the 1×10^{15} He ions/cm^2 dosed sample, consisting of a low order and a high order component. Note f_1 is the number fraction corresponding to the low order component (refer to the Appendix for fitting methodology).

3.3.4. Mechanisms associated with the ~1000 °C desorption event

The high order component of this event (sharp peak) is believed to result from the $\alpha\leftrightarrow\gamma$ phase transition. First, the repetitive appearance of this sharp component during successive heating–cooling cycles resembles the reversibility of the phase transition very well. Without the reversible phase transition, we can only expect a monotonically decreasing desorption rate without any peaks during cooling since both the reaction constant $K_0\exp(-Q/K_BT)$ and the remaining number of desorbing species N in the rate equations (any order) decrease as temperature decreases. Second, considering that the JMA model is primarily applicable to phase transitions, the success of the JMA model in reproducing the sharp component provides another supportive evidence for the claim. It should be mentioned that the JMA model is limited to diffusional phase transitions proceeding by nucleation and growth and it cannot describe diffusionless martensitic phase transition. However, the martensitic phase transition can occur in elemental iron only at extremely high cooling rates on the order of 10^4 K/s [26], far above the rates in this study. Sugano et al. [27] and Ono et al. [28] have also reported the observation of non-first-order rapid release signals from helium-implanted iron and ferritic alloys and attributed them to phase transitions.

Noticing the similarity between the 3.8 eV obtained in the present experiment and the 3.9 eV obtained for HeV (substitutional helium) dissociation energy by Berg et al. [29] and Morishita et al. [10] in simulations, it is tempting to attribute the low order component of the ~1000 °C event to the dissociation of HeV clusters. However, further investigations are required to confirm this.

We did not analyze the desorption signal at even higher temperatures (above 1100 °C) since we are mainly interested in comparing the experiment with simulations in BCC iron.

3.4. Samples of 1×10^{13} and 1×10^{11}/cm^2 dose

The ~1000 °C desorption event observed for the 1×10^{15} He/cm^2 samples was not unambiguously observed from the 1×10^{11} and 1×10^{13} He/cm^2 samples for the same heating ramp conditions. Rather, these lower dose samples exhibited very similar signals (spurious peaks) to the non-implanted samples. The absence of strong desorption signals from these two samples may not be a surprise since the total number of implanted He atoms in these samples is much lower than the 1×10^{15} He/cm^2 samples. It appears necessary to improve the signal to background ratio of the system in order to successfully detect any desorption events occurring in these lower dose samples, in addition to performing the implantations at lower He ion energies.

4. Conclusions

He desorption from iron implanted with 100 keV He to a dose of 1×10^{15} He/cm^2 occurs mainly at high temperatures (above 880 °C). Two major desorption events have been observed for this sample during constant rate (1 K/s) heating: one with a fully developed peak at 1017 °C, the other with an onset of ~1100 °C, but not fully developed up to 1330 °C. Analysis based on conventional reaction model and JMA transformation model reveals that the 1017 °C event of the 1×10^{15} He/cm^2 sample comprises two components, a low order ($n \sim 1.1$) and a high order ($n \sim 5.8$, JMA model), with the same activation energy of ~3.8 eV. The high order component is ascribed to the $\alpha \leftrightarrow \gamma$ phase transition based on the success of JMA model in data reproduction and on its repetitive appearance in heating–cooling cycles, while the low order component is likely to be related to the dissociation of HeV clusters comparing the activation energies determined here and in computer simulations. He desorption signals from the 1×10^{11} and 1×10^{13} He/cm^2 (100 keV) implanted samples have not been successfully detected at present. Spurious peaks that demand special attention in future THDS data analysis are reported.

Appendix

Methodology for the two-order JMA fit (shown in Fig. 4) for the 1017 °C desorption event of the 100 keV, 1×10^{15} He/cm^2 dosed iron:

(i) $N_{01} = f_1 * N_0$ and $N_{02} = (1 - f_1) * N_0$;
(ii) $\mathrm{d}N/\mathrm{d}t = \mathrm{d}N_1/\mathrm{d}t + \mathrm{d}N_2/\mathrm{d}t$;
(iii) $\mathrm{d}N_i/\mathrm{d}t = -N_{0i} * \mathrm{d}x_i/\mathrm{d}t = -N_{0i} * n_i K_i^{n_i} t^{n_i - 1} \times \exp(-K_i^{n_i} t^{n_i}) * [1 + \beta * tQ_i/(K_B T^2)]$ $(i = 1,2)$;
(iv) $K_i = K_{0i} \exp(-Q_i/K_B T)$ $(i = 1,2)$,

where f_1 is the number fraction corresponding to the low order component, and N_0 is the total number of He atoms for the entire desorption event.

References

[1] E.E. Bloom, F.W. Wiffen, J. Nucl. Mater. 58 (1975) 171.
[2] L.K. Mansur, W.A. Coghlan, J. Nucl. Mater. 119 (1983) 1.
[3] H. Ullmaier, Nucl. Fus. 24 (1984) 1039.
[4] L.K. Mansur, M.L. Grossbeck, J. Nucl. Mater. 155 (1988) 130.
[5] H. Trinkaus, B.N. Singh, J. Nucl. Mater. 323 (2003) 229.
[6] A.V. Fedorov, A. van Veen, A.I. Ryazanov, J. Nucl. Mater. 233 (1996) 385.
[7] E. Oliviero, M.F. Beaufort, J.F. Barbot, A. van Veen, A.V. Fedorov, J. Appl. Phys. 93 (2003) 231.
[8] I. Mori, T. Morimoto, R. Kawakami, K. Tominaga, Nucl. Instrum. and Meth. B 153 (1999) 126.
[9] A.A. Selezenev, V.G. Golubev, N.S. Ganchuk, Chem. Phys. Rep. 17 (1998) 295.
[10] K. Morishita, R. Sugano, B.D. Wirth, T.D. de la Rubia, Nucl. Instrum. and Meth. B 202 (2003) 76.
[11] R.J. Kurtz, H.L. Heinisch, J. Nucl. Mater. 329 (2004) 1199.
[12] C.C. Fu, J.D. Torre, F. Willaime, J.L. Bocquet, A. Barbu, Nat. Mater. 4 (2005) 68.
[13] M.B. Lewis, K. Farrell, Nucl. Instrum. and Meth. Phys. Res. B 16 (1986) 163.
[14] K. Arakawa, R. Imamura, K. Ohota, K. Ono, J. Appl. Phys. 89 (2001) 4752.
[15] T. Ishizaki, Q. Xu, T. Yoshiie, S. Nagata, Mater. Trans. 45 (2004) 9.
[16] T. Iwai, Y. Ito, M. Koshimizu, J. Nucl. Mater. 329 (2004) 963.
[17] R. Sugano, K. Morishita, A. Kimura, H. Iwakiri, N. Yoshida, J. Nucl. Mater. 329 (2004) 942.
[18] R. Vassen, H. Trinkaus, P. Jung, Phys. Rev. B 44 (1991) 4206.
[19] S. Takaki, J. Fuss, H. Kugler, U. Dedek, H. Schultz, Radiat. Eff. 79 (1983) 87.
[20] S.C. Glade, B.D. Wirth, H. Schut, Fusion Materials Semi-Annual Progress Reports, DOE/ER-0313/37, 2004, 136.
[21] J.F. Ziegler, J.P. Biersack, U. Littmark, The Stopping and Range of Ions in Matter, Pergamon, New York, 1984.
[22] A. van Veen, A. Warnaar, L.M. Caspers, Vacuum 30 (1980) 109.
[23] W.A. Johnson, R.F. Mehl, Trans. Am. Inst. Min. Metall. Eng. 135 (1939) 416.
[24] M. Avrami, J. Chem. Phys. 7 (1939) 1103.
[25] D.W. Henderson, J. Non-Cryst. Solids 30 (1979) 301.
[26] ASM Handbook, ASM International, vol. 9, 148 (2004).
[27] R. Sugano, K. Morishita, A. Kimura, Fus. Sci. Technol. 44 (2003) 446.
[28] K. Ono, K. Arakawa, H. Shibasaki, H. Kurata, I. Nakamichi, N. Yoshida, J. Nucl. Mater. 329–333 (2004) 933.
[29] F.v.d. Berg, W.v. Heugten, L.M. Caspers, A.v. Veen, Solid State Commun. 24 (1977) 193.